Detection of Myocardial Scar from the VCG using a Supervised Learning Approach

Christos Panagiotou[1], Sofia-Maria Dima[1], Evangelos B. Mazomenos[2], James Rosengarten[3], Koushik Maharatna[2], John Gialelis[1], John Morgan[3]

***Abstract*— This paper addresses the possibility of detecting presence of scar tissue in the myocardium through the investigation of vectorcardiogram (VCG) characteristics. Scarred myocardium is the result of myocardial infarction (MI) due to ischemia and creates a substrate for the manifestation of fatal arrhythmias. Our efforts are focused on the development of a classification scheme for the early screening of patients for the presence of scar. More specifically, a supervised learning model based on the extracted VCG features is proposed and validated through comprehensive testing analysis. The achieved accuracy of 82.36% (sensitivity 84.31%, specificity 77.36%) indicates the potential of the proposed screening mechanism for detecting the presence/absence of scar tissue.**

***Index Terms*— VCG, myocardial scar, SVM classification**

I. INTRODUCTION

Fatal arrhythmias (ventricular tachycardia/fibrillation), mostly caused due to disordered conduction from injured heart tissue known as scar, is the leading cause of sudden cardiac death (SCD). Myocardial scar is the end result of myocardial infarction (MI) which is caused from insufficient blood supply to a part of the heart (ischemia). This leads to the death of a portion of cardiac cells (scarred tissue) and affects the contractile properties of the myocardium. The standard methods to accurately determine the scar's presence, size and location are imaging techniques like Cardiac Magnetic Resonance Imaging (CMR). The main drawback of CMR is its limited availability due to high cost, both in terms of resources and specialized personnel. In addition, CMR lacks portability. Therefore novel methods, with high portability thus capable to be applied in the point-of-care, should be developed in order to provide a screening system for the initial identification of scar tissue in patients who have suffered MI, in a fast, inexpensive and accurate manner.

Such techniques could be developed based on the electrocardiogram (ECG), the most widespread method for monitoring the heart. Research conducted in parallel with the ECG introduced the concept of a vector quantity that could describe the heart's electrical activity. That concept initiated the field of vectorcardiography and the vectorcardiogram (VCG). VCG recordings require their own lead system and among the various proposed systems, Frank's orthogonal leads [1], based on the human torso model [2], [3], became the standard for capturing the VCG. In essence, the VCG carries the same electrical information as the ECG but it is less intrucive since it requires only 3 leads. Furthermore its vectorial representation, gives additional spatial characteristics that can enhance the analysis of the heart's functionality [4]. Fig. 1 illustrates an ECG heartbeat and the respective VCG. As an example of VCG utilization we refer to [5], where the authors attempt to classify healthy subjects and MI patients using a set of features based on the planarity of the T-wave loop from the VCG. However the limited set of records does not allow a concrete evaluation of the system's robustness.

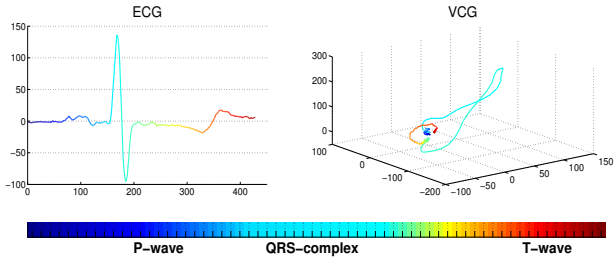

Fig. 1: The ECG and the VCG for the same single beat.

In this paper we study the VCG, the resultant from the magnitude and direction of the electrical forces, generated during the cardiac cycle and we observe how it evolves in time on the 3D space of the VCG. From the spatial analysis of the VCG we extract a number of features, which we hypothesize that they capture the differences of the heart's activity when scar tissue is present/absent. We then formulate a classification mechanism, based on a set of 27 features. The proposed system is evaluated exhaustively over healthy and scarred records. The rest of this paper is organized as follows. In Section II we present our methodology and the extracted VCG features, while in Section III the classification and feature selection workflow are described. The results of our experiments are presented and discussed in Section IV while conclusions are drawn in Section V.

II. METHODOLOGY

The formation of scarred tissue due to MI affects the propagation of the electrical stimuli of the heart with fatal

This work was supported by E.U. ARTEMIS Joint Undertaking under the Cyclic and person-centric Health management: Integrated appRoach for hOme, mobile and clinical eNvironments - (CHIRON) Project, Grant Agreement # 2009-1-100228.

[1] C.Panagiotou, S.M.Dima, J.Gialelis are with Industrial Systems Institute, ATHENA RC, Platani, Patras, 265 04, GR. (email:panagiotou,sdima,gialelis@isi.gr)

[2]E. B. Mazomenos, K. Maharatna are with School of Electronics and Computer Science, University of Southampton, Southampton, SO17 1BJ, UK. (e-mail: ebm, km3@ecs.soton.ac.uk)

[3]J. Rosengarten, J. Morgan are with University Hospitals Southampton NHS Trust, SO17 1BJ, UK. (e-mail: james@rosengarten.co.uk, jmm@hrclinic.org

arrhythmias being the consequences of that disordered conduction. Scar tissue cannot get properly excited and results in the electrical stimuli following more than one conduction pathways with different conduction velocities, that ultimately causes conduction delays. This may lead to the generation of the re-entry phenomenon which if repeated perpetually may lead to SCD [6] . In the ECG trace, scar tissue causes alterations in the QRS-complex characteristics, such as the value of QRS-angle, R-wave prolongations and presence of fragmentations [7], [8]. The morphology of the T-wave is also know to be affected, since it represents the repolarization of the ventricles [9].

In the present work we claim that scar-related delayed conduction can be also reflected to a set of spatial features extracted from the VCG. In order to justify our hypothesis we extracted a set of features that were then used as an input to a classifier. Clinical cardiology dictates that alterations caused by the presence of scar tissue on the ECG and the VCG will be present on every single heartbeat, therefore features are extracted from the VCG of a single PQRST complex. Since, there is poor utilization of the VCG in clinical practice, records with independently recorded VCG from Frank's orthogonal leads are rare. Nevertheless many efforts focused on reconstructing the 12-lead ECG from VCG and vice versa. The most clinically accepted method is attributed to Dower and for the purpose of our work we employed the inverse Dower matrix transformation [10], in situations where the VCG was not directly recorded. Dower's matrix consists of lead specific coefficients, used to calculate the eight independent leads (V1-V6, I and II) as a linear combination of the VCG. The inverse process produces the VCG leads from the 12-lead ECG. The 3×8 inverse Dower matrix (iD) is given as:

$$\begin{bmatrix} -0.172 & -0.074 & 0.122 & 0.231 & 0.239 & 0.194 & 0.156 & -0.010 \\ 0.057 & -0.019 & -0.106 & -0.022 & 0.041 & 0.048 & -0.227 & 0.887 \\ -0.229 & -0.310 & -0.246 & -0.063 & 0.055 & 0.108 & 0.022 & 0.102 \end{bmatrix}$$

$$L = [\ V1 \quad V2 \quad V3 \quad V4 \quad V5 \quad V6 \quad I \quad II\ ]^T$$

$$VCG = [\ VCGx \quad VCGy \quad VCGz\ ]^T$$

$$VCG = L \times iD \tag{1}$$

The preprocessing steps required for the VCG analysis, are the ECG baseline removal, accomplished following the methodology presented in [11] and the ECG waves boundaries determination accomplished using the TDMG delineator presented in [12]. From the VCG (recorded or reconstructed) we extract a set of spatial features we believe may reflect the effects of delayed conduction on the VCG morphology. Our focus is on the QRS-complex and the T-wave and the extracted features are vector and area related. The use of the TDMG delineator allows us to determine the temporal boundaries of the QRS-complex loop (QRS-loop) and T-wave loop (T-loop) in the VCG. These are obtained from the maximum QRS- and T-duration after applying TDMG on the ECG leads. Having localised the QRS- and T-loops in the VCG, allows us to define the peak point of these loops (R-peak, T-peak) as the point with maximum distance from the origin. In addition we extract the vectors of maximum width, (R-width, T- width) in the QRS- and T-loop, defined by the two points which demonstrate the maximum distance in each loop. For each vector we calculate the magnitude and angle. Additionally the centroid point of the VCG that represents its geometric center and defined as $C = \frac{\int xg(x)\mathrm{dx}}{\int g(x)\mathrm{dx}}$, is extracted and the respective vector along with its magnitude and angle are calculated. Finally we calculate the area of the VCG curve by counting the number of pixels enclosed by it. The set of features is summarized in the following list and depicted on Fig. 2:

- R-width, T-width magnitude
- R-peak, T-peak & Centroid vector magnitudes
- R-peak T-peak & Centroid vector angles
- VCG areas

These features are calculated for each of the projections of the 3D VCG, of a single heartbeat, on the three planes (XY-XZ-YZ). The 27 extracted parameters consist the VCG Feature space (VCG-FS) of our investigation.

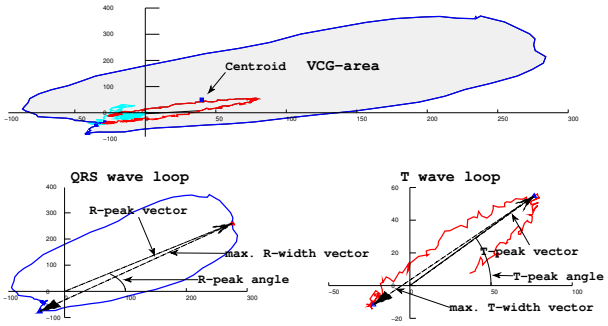

Fig. 2: VCG extracted features from XY plane.

In our experimentation we used ECG records from two sources: the Cardiology Department of the University Hospital Southampton NHS Trust (UHS-NHS) and the PTB Diagnostic ECG Database (PTDB) available in Physionet [13]. Two databases (DB-I/II) are provided by the UHS-NHS. These constitute of subjects which had 12-lead ECGs and CMR measurements performed within the same period. The CMR examination provides the size (in terms of %) of the scarred tissue. From the CMR results we are able to define the class for each instance by considering a 0% CMR measurement as absence of scar and anything >0% as presence. The first database (DB-I) consists of 154 records with 108 of them having verified scar tissue, while the remaining 46 do not have scar. The sampling frequency is 500Hz while the A/D resolution is 2.5641 μV. The second database (DB-II) consists of 54 patients, where only 4 are free of scar. The sampling frequency is 1kHz and the A/D resolution is 0.5μV. In the DB-I and DB-II samples Frank's leads were not recordede and therefore we utilized the iD transformation for the VCG construction. In order to balance our dataset and to test the capability of our system to correctly classify no-scar instances, we utilized a third database (DB-III). This was

obtained from the 52 healthy control records of the PTBDB. Although PTBDB does not provide any CMR results, the annotation of these records as healthy controls, allowed us to imply that no scarred tissue is present. Moreover, PTBDB includes actual measurements of Frank's XYZ orthogonal leads, therefore there was no need for VCG reconstruction through iD transformation. The frequency and the resolution are the same as (DB-II). In total 260 records were considered with 158 records having CMR verified scarred tissue.

III. CLASSIFICATION

The extracted features from the processing of the VCG were used to formulate a robust classification model, able to discriminate the presence/absence of myocardial scar, following a supervised learning approach. The classification algorithm that is utilized is the Support Vector Machine (SVM) [14]. Analysis was facilitated by employing the Weka machine learning software. The two options for estimating the performance of a derived classification model are the hold out and the cross validation (CV) procedure. In the first one, records are randomized and divided into two sets: the training set which is the 2/3 of the dataset and the test set which is the remaining 1/3. Firstly the classification model is built, extracting the knowledge from the training records and then this knowledge is applied on the test instances, so as to evaluate the classification rate. However, the disadvantages of this method is that the accuracy is estimated based on a single random partitioning, which may not be indicative of the model's actual performance. In the 10 fold-CV case the dataset is randomized and is divided into 10 mutually exclusive parts, with almost the same number of data instances for each one. The 10 fold-CV strategy consists of 10 experiments. In the i-th (i=1,.. .10) experiment the i-th fold is used as testing set, while the remaining 9 folds are merged and used as training set. The average accuracy of the 10 runs experiments provides the overall accuracy of the model. To obtain a more valid estimation of the model's performance multiple runs of the 10 fold-CV are required, where the initial dataset is randomized in each run. To avoid the stratification problem the number of instances for the two classes is balanced in CV experiments. The actual performance of the classification system in real applications, is determined when an already trained classifier is applied on records with different characteristics preferably obtained from a different database.

When investigating a set of features for classification purposes, the feature's space dimensionality reduction is a common strategy for identifying features that may add redundancy and thus reduce the classification accuracy. The process of feature selection also gives an insight into the relative importance of each of the features for the particular classification task. In our work, several feature selection algorithms have been tested such as Information Gain, Relief and SVM Attribute Evaluation (SVMAttributeEval [15]). The utilization of SVMAttributeEval gave us the optimal performance. SVMAttributeEval is implemented with the Ranker search method which evaluates the importance of a feature by using an SVM classifier.

TABLE I: Evaluation Results

Metric	Performance%	Details (number of training records for each class)	Feature Space
Acc	69.56%	10 fold CV	
Sens	71.74%	balanced DB-I (46-46)	VCG
Spec	67.39%	**(Exp-I)**	
Acc	71.45%	10 fold CV	
Sens	73.91%	balanced DB-I (46-46)	VCG-RFS
Spec	63.04%	**(Exp-II)**	
Acc	85.85%	Train with balanced DB-I (46-46)	
Sens	88.00%	Test on DB-II/III	VCG-RFS
Spec	83.93%	**(Exp-III)**	
Acc	70.83%	Train with balanced DB-I (46-46)	
Sens	64.29%	Test on the remaining of DB I and DB-II/III	VCG-RFS
Spec	83.93%	**(Exp-IV)**	
Acc	82.36%	10 fold CV	
Sens	84.31%	Balanced DB-I/II/III (102-102)	VCG-RFS
Spec	77.36%	**(Exp-V)**	

DB-I: 108 scar records, 46 no-scar records (VCG reconstructed from iD)
DB-II: 50 scar records, 4 no-scar records (VCG reconstructed from iD)
DB-III: 52 no-scar records (recorded VCG)

The performance metrics we utilize are: the classification accuracy (Acc), the specificity (Spec) and sensitivity (Sens). Subsequently we define as True Positive(TP)/False Negative(FN) the records that have scar and are correctly/incorrectly identified, while False Positive(FP)/True Negative (TN) the records that do not have scar and are incorrectly/correctly classified. $Sens = \frac{TP}{TP+FN}$ $Spec = \frac{TN}{TN+FP}$ $Acc = \frac{TP+TN}{FN+FP+TP+TN}$

IV. RESULTS

Performance results from our experimentation are listed in Table I. In Exp-I, a balanced dataset from DB-I is constructed, using 46 records for each class. For the scar class the 46 records with the higher scar size are selected. The results when using the entire VCG-FS (69.56% Acc and 71.74% Sens and 67.39% Spec) indicate that both classes can be sufficiently distinguished. However, we attempt to improve the classification model, by using the SVMAttributeEval feature selection algorithm and reduce the feature space to 10 attributes (VCG-RFS), with which, the best classification accuracy is achieved. Features are ranked according to the square of the weight assigned to them by the SVM. Based on these weights we selected the top 10 since the rest have weights with lower impact and do not contribute to the classification process. Exp-II is a similar experiment to Exp-I, but with feature selection applied. The classification rate in Exp-II slightly improves to 71.45%. The top 10 selected features are, T-peak angle, R-peak angle, T-peak magnitude and T-width magnitude in the XY plane, T-peak magnitude, R-peak angle, T-width magnitude, VCG-area and R-peak magnitude in YZ plane and finally R-peak angle in the XZ plane. The significance of the R- and T-angle in the XY plane is depicted in Fig. 3, which is a 2D scatter plot of these two features and where we observe that the two classes are distinguishable. This is also justified in Fig. 4, which presents the R- and T-peak angles of a scar and a no-scar VCG record.

To validate the effectiveness of our classification model, we test it on databases with different characteristics. For that purpose, in Exp-III we used the classification model, generated in Exp-II and tested it on DB-II and DB-III

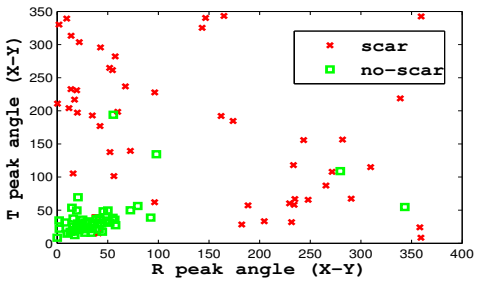

Fig. 3: Scatter Plof of R- and T-peak angle (XY)

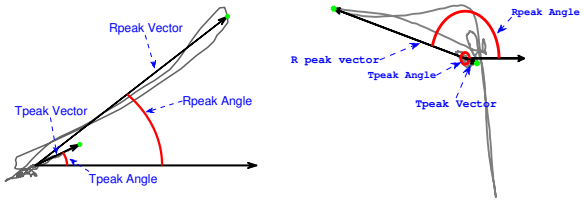

Fig. 4: R- and T-peak angle in No-Scar(left) and Scar(right) VCG

records. The high performance results (Acc-85.85%) indicate that our system is able to detect the presence of scar, also in databases with different characteristics. Moreover in Exp-IV, we extend Exp-III, by adding the remaining records from DB-I as testing records. The accuracy and sensitivity are decreased (Acc-70.83%), while the specificity remains in the same levels. This means that records with scar are not classified sufficiently. In our opinion, this is attributed to the fact that the remaining records from DB-I are the records with the lower scar size, since as we mentioned before, records with the highest percentage of scar were used in the training phase. To illustrate this, the testing records that have scar in Exp-IV are grouped into 4 groups, based on the scar size value obtained through CMR. As depicted in Fig. 5 the number of False Negatives decreases, as the scar size increases. From this analysis we conclude that records with high scar size can be effectively labeled with the proposed system, as in the training step records with high scar size are used. The dashed line in the Fig. 5 is the average error of 35.71% (1-Sens) and shows which of the four groups are closer to that in Exp-IV. Finally in order to obtain a comprehensive view of our model we conducted an experiment (Exp-V), where we merge all three DBs and construct a balanced dataset from all available records. As the number of no-scar records is 102 (158 records have scar), we construct a dataset of 204 instances and apply 10 runs of 10 fold CV, using the reduced feature space (VCG-RFS). The performance of Exp-V (Acc: 82.36%) indicates that our model can sufficiently detect the presence of scar. It is to be noted that the obtained performance will inherently be affected by errors introduced by the reconstruction of the VCG through the iD transformation.

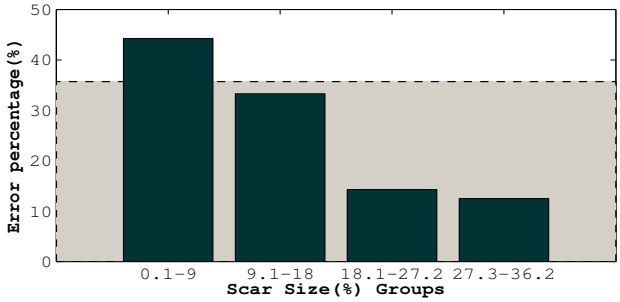

Fig. 5: Misclassified scar records in Exp-IV

V. CONCLUSIONS

This paper addresses the problem of detecting the presence/absence of myocardial scar from standard ECG/VCG recordings. In that context, a classification model, based on the VCG's spatial characteristics, is proposed. A set of 27 features, not considered before for that purpose, are generated in order to capture the effects caused by the presence of scar in the heart's electrical activity. Based on these a comprehensive investigation has been conducted on the selected features, using a SVM based classifier. Prominent performance is achieved even though the uncertainty introduced by the inverse Dower transformation. The classification rate of 82.36% along with the sensitivity (84.31%) and specificity metrics (77.36%) indicate that our proposed model can be utilized in a non-invasive system for the initial screening of presence/absence of myocardial scar.

REFERENCES

[1] E. Frank, "An accurate, clinically practical system for spatial vectorcardiography," *Circ.*, vol. 13, no. 5, pp. 737–749, 1956.
[2] ——, "A direct experimental study of three systems of spatial vectorcardiography," *Circ.*, vol. 10, no. 1, pp. 101–113, 1954.
[3] E. Frank and C. F. Kay, "Frontal plane studies of homogeneous torso models," *Circ.*, vol. 9, no. 5, pp. 724–740, 1954.
[4] T.-C. Chou, "When is the vectorcardiogram superior to the scalar electrocardiogram?" *J Am Coll Cardiol*, vol. 8, no. 4, 1986.
[5] Karsikas *et al.*, "New vectorcardiographic non-planarity measure of t-wave loop improves separation between healthy subjects and myocardial infarction patients," in *IEEE EMBC*, 2009, pp. 1754 –1757.
[6] R. Baltazar, *Basic and Bedside Electrocardiography*, ser. LWW medical book collection. Lippincott Williams & Wilkins, 2009.
[7] R. H. Selvester *et al.*
[8] ——, "Analog computer model of the vectorcardiogram," *Circ.*, vol. 31, no. 1, pp. 45–53, 1965.
[9] S. M. Narayan *et al.*, "Relation of t-wave alternans to regional left ventricular dysfunction and eccentric hypertrophy secondary to coronary heart disease," *Am Heart J.*, vol. 97, no. 6, 2006.
[10] D. GE *et al.*, "On deriving the electrocardiogram from vectoradiographic leads." *Clinical cardiology*, vol. 3, no. 2, pp. 87–95, 1980, review,.
[11] P. de Chazal *et al.*, "Automatic classification of heartbeats using ECG morphology and heartbeat interval features," *IEEE Trans. Biomed. Eng.*, vol. 51, no. 7, pp. 1196 –1206, Jul 2004.
[12] E. Mazomenos *et al.*, "A time-domain morphology and gradient based algorithm for ecg feature extraction," in *2012 IEEE ICIT*, Mar 2012, pp. 117 –122.
[13] http://www.physionet.org/physiobank/database/ptbdb/.
[14] A. Christmann and I. Steinwart, *Support Vector Machines*, ser. Information Science and Statistics. Springer, 2008.
[15] Guyon *et al.*, "Gene selection for cancer classification using support vector machines," *Mach. Learn.*, vol. 46, no. 1-3, pp. 389–422, 2002.